Unconventional superconducting states of interlayer pairing in bilayer and trilayer graphene

Mir Vahid Hosseini and Malek Zareyan
Department of Physics, Institute for Advanced Studies in Basic Sciences (IASBS), Zanjan 45137-66731, Iran
(Received 4 October 2012; published 6 December 2012)

We develop a theory for interlayer pairing of chiral electrons in graphene materials which results in an unconventional superconducting state with an s-wave spin-triplet order parameter. In a pure bilayer graphene, this superconductivity exhibits a gapless property with an exotic effect of temperature-induced condensation causing an increase of the pairing amplitude with increasing temperature. We find that a finite doping opens a gap in the excitation spectrum and weakens this anomalous temperature dependence. We further explore the possibility of realizing a variety of pairing patterns with different topologies of the Fermi surface, by tuning the difference in the doping of the two layers. In trilayer graphene, the interlayer superconductivity is characterized by a two-component order parameter which can be used to define two distinct phases in which only one of the components is nonvanishing. For *ABA* stacking the stable state is determined by a competition between these two phases. On variation of the relative amplitude of the corresponding coupling strength, a first-order phase transition can occur between these two phases. For *ABC* stacking, we find that the two phases coexist with the possibility of a similar phase transition, which turns out to be second order.

DOI: 10.1103/PhysRevB.86.214503 PACS number(s): 74.78.−w, 74.70.Wz, 73.22.Pr

I. INTRODUCTION

The microscopic theory of superconductivity developed by Bardeen, Cooper, and Schrieffer[1](BCS) is based on the pairing between electrons from opposite-spin subbands with the same Fermi surfaces. Generalization of the BCS pairing to composite systems of two (or more) types of fermions with different Fermi surfaces[2] has attracted great interest due to its appearance in various areas of physics, including pairing of ultracold Fermi atoms,[3,4] color superconductivity in dense quark matter,[5] and neutron-proton pairing in nuclear systems.[6] Despite the robustness of conventional metallic superconductivity[7] against small mismatches between the paired Fermi surfaces, several unconventional pairing phases have been predicted to occur in the presence of larger mismatches. The best-known cases include the phase of breached pairing, referring to a state of separated normal (N) and superconducting (S) phases in the momentum space,[8] pairing between deformed Fermi surfaces with zero total momentum of Cooper pairs,[9] and the inhomogeneous S Larkin-Ovchinnikov-Fulde-Ferrel (LOFF) phase.[10] These unconventional phases result from different topologies of the Fermi surface.

The search for new exotic S states is a subject at the frontier of low-temperature physics research, because it sheds light on the pairing symmetry and may lead to an understanding of the pairing mechanism of superconductivity in high-T_c superconductors[11] and other newly discovered S materials.[12] The recent discoveries of graphene,[13,14] the two-dimensional solid of carbon atoms with honeycomb lattice structure, and its associated bilayer and trilayer structures are expected to provide a further opportunity for realizing unconventional pairing states. Graphene has a specific zero-gap electronic band structure in which the charge carriers behave like two-dimensional (2D) massless Dirac fermions with a pseudorelativistic chiral property. In addition to regular spin, electrons in graphene possess two additional quantum degrees of freedom, the so-called pseudospin and valley. These features, together with the fact that in graphene the carrier type [electronlike (n) or holelike (p)] and its density can be tuned conveniently, make these carbon-based material exceptional for realizing unconventional superconductivity. The unusual features of superconductivity have already been predicted in monolayer graphene,[15] where the pairing of electrons with opposite sublattice pseudospins leads to the appearance of an unusual spin-singlet $(p+ip)$-wave S phase with no gap in its excitation spectrum.[16] An intrinsic superconductivity, with plasmon- or phonon-mediated pairing interactions, can be realized in graphene coated with a metal.[16,17] For a coated bilayer or trilayer graphene, the formation of the S state is expected to be closely similar to that of graphite intercalated with alkaline-earth metals, for which a critical temperature up to 11.5 K has been reported.[18] Furthermore, progress has already been made in proximity-induced superconductivity by fabrication of transparent contacts between a graphene monolayer and a superconductor (see, for instance, Refs. 19). In a very recent study,[20] we have explored the exotic nature of interlayer superconductivity in pure bilayer graphene. The mechanism by which the interplay between the interlayer pairing of electrons with the same sublattice chirality and the asymmetric arrangement of the sublattices of the two layers results in a gapless superconductivity with an unusual s-wave spin-triplet symmetry of the order parameter and anomalous thermodynamic properties was explained. We obtained the result that the interlayer pairing allows for the possibility of a temperature-induced condensation causing an increase of the pairing amplitude (PA) with increasing temperature, and an entropy of the stable S state which can be higher than its value in the N state. Motivated by these findings for the interlayer superconductivity of pure bilayer graphene, we study the effect of finite doping. Furthermore, considering the recent interest in the properties of trilayer graphene,[21,22] we extend our study to the interlayer pairing in trilayer graphene. For bilayer graphene, we find that the doping opens a gap in the excitation spectrum which, in turn, weakens the temperature-induced condensation such that at high levels of the doping the temperature dependence of the PA becomes

similar to that of the conventional BCS gap.[7] We present phase diagrams of interlayer superconductivity for both symmetric and asymmetric doping, with the two layers having the same and different levels of doping, respectively.

For trilayer graphene, we examine the interlayer pairing in two different types of stacking, *ABA* and *ABC*, in the pure case and find a strong dependence on the type of stacking. We show that the asymmetric *ABC* stacking can support a stronger pairing gap than the symmetric *ABA* stacking. For *ABA* stacking, there is a competition between two phases of interlayer superconductivity in which the pairing is realized between chiral electrons of the middle layer and those in only one of the other two layers. This depends on the relative values of the two corresponding coupling strengths. We explore the possibility of a phase transition between the two phases by varying the coupling strength; the transition turns out to be first order for *ABA* stacking but second order for *ABC* stacking.

The paper is organized as follows. In the next section, we discuss the theoretical modeling of the interlayer superconductivity in graphene materials and study the resulting band structure with different topologies of the Fermi surfaces. In Sec. III, we discuss the numerical results for the phase diagram and the order parameter as a function of the various parameters of both symmetrically and asymmetrically doped bilayer graphene. Section IV is devoted to the case of interlayer superconductivity for trilayer graphene. Finally, in Sec. V, we present our summary and conclusions.

II. THEORY

In order to study interlayer superconductivity, we consider a model based on graphene materials. We introduce the theory of interlayer superconductivity for the case of bilayer graphene and then this theory is developed for the case of trilayer graphene. Bilayer graphene is composed of two coupled graphene monolayers with A_1 and B_1 triangular sublattices in the top layer and A_2 and B_2 triangular sublattices in the bottom layer, according to Bernal stacking in which every A_1 site of the top layer lies directly above a B_2 site of the bottom layer. In the absence of superconductivity, the following Hamiltonian can be used to describe the π electrons of bilayer graphene:[23]

$$H_0^{AB} = \sum_{l=1}^{2} H_l^{\text{mono}} + H_\perp^{AB}, \tag{1}$$

with the monolayer Hamiltonian

$$H_l^{\text{mono}} = -\sum_{\sigma,i} \mu_l n_{l,i,\sigma} - t \sum_{\sigma,\langle i,j\rangle} (a_{l,i,\sigma}^\dagger b_{l,j,\sigma} + \text{H.c.}), \tag{2}$$

and the nearest-neighbor interlayer hopping Hamiltonian

$$H_\perp^{AB} = -t_\perp \sum_{\sigma,i} (a_{1,i,\sigma}^\dagger b_{2,i,\sigma} + \text{H.c.}), \tag{3}$$

where $a_{l,i,\sigma}$ ($b_{l,i,\sigma}$) and $a_{l,i,\sigma}^\dagger$ ($b_{l,i,\sigma}^\dagger$) are the annihilation and the creation operators of an electron in the ith unit cell in the sublattice A (B) and the layer l. $\sigma = \pm$ denotes the spin state of the electron; $n_{l,i,\sigma}$ is the corresponding on-site particle density operator. The intralayer nearest-neighbor hopping energy $t \approx 3$ eV determines the Fermi velocity in graphene as $v_F \approx 10^6$ m/s, and $t_\perp \approx 0.4$ eV ($t_\perp/t \approx 0.13$) is the dominant interlayer hopping energy between the nearest neighbors A_1 and B_2; the chemical potential μ_l can be controlled by top- and bottom-gate electrodes independently.

By introducing an attractive interaction between the electrons of the sublattices A_1 and B_2 through the following potential:

$$V_\perp^{AB} = -g_{\perp 1} \sum_{\sigma,\sigma',i} a_{1,i,\sigma}^\dagger a_{1,i,\sigma} b_{2,i,\sigma'}^\dagger b_{2,i,\sigma'}, \tag{4}$$

interlayer superconductivity can be produced. Here, $g_{\perp 1}$ is the S coupling energy.[17,24] The interaction potential (4) has the on-site local properties in the 2D plane of the bilayer graphene. Therefore, the wave function of the two-body problem associated with the two coupled electrons and the corresponding pairing potential are not extended in the bilayer plane. This results in the introduction of isotropic s-wave symmetry for the orbital part of the order parameter. Because the coupling occurs between two electrons with opposite pseudospin degrees of freedom, the Pauli exclusion principle imposes a pairing in the spin-triplet channel. Therefore, the total wave function, including the product of orbital, spin, and pseudospin parts, will be antisymmetric under the exchange of electrons. The following s-wave spin-triplet order parameter can be used to decouple the total Hamiltonian of the bilayer graphene ($H^{AB} = H_0^{AB} + V_\perp^{AB}$):

$$\Delta_{i,\perp 1} = -g_{\perp 1} \langle a_{1,i,\downarrow} b_{2,i,\uparrow} + a_{1,i,\uparrow} b_{2,i,\downarrow} \rangle. \tag{5}$$

In the lattice space, as is shown in the left panel of Fig. 1, $\Delta_{i,\perp 1}$ describes the interlayer pairing of the two electrons in the sublattices A_1-B_2, and the spins $\uparrow$-$\downarrow$ (and $\downarrow$-$\uparrow$). In the momentum space, for the case of $t_\perp = 0$, when the electronic band structures of the two monolayers are not affected by each other, there is a simple description for binding of the

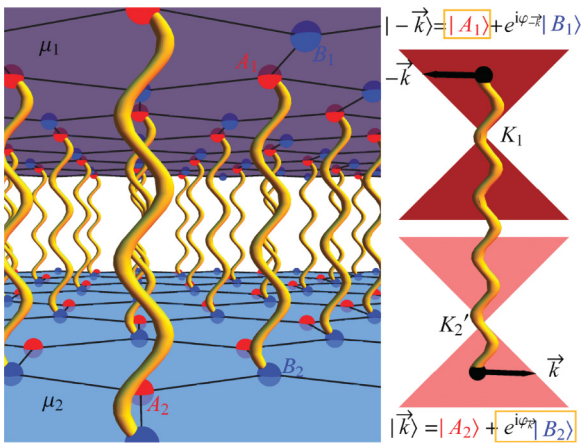

FIG. 1. (Color online) Left panel: Lattice structure of bilayer graphene. Interlayer S correlations in real space are shown by wavy lines which couple electrons of different layers with opposite pseudospin degrees of freedom. Right panel: Interlayer superconductivity in momentum space is shown by coupling of two time-reversed momentum states $|-k\rangle$ and $|k\rangle$ which are located in valleys K_1 and K_2' and belong to different layers. Since interlayer pairing is antisymmetric with respect to the pseudospin degree of freedom, pairing between components $|A_1\rangle$ and $|B_2\rangle$ is possible.

two time-reversed electronic states due to the presence of an attractive interaction, as we discuss in the following.

At low energies, the chiral momentum states $|k\rangle$ located in Dirac cone-shaped band structures in the two inequivalent valleys are coherent superpositions of sublattice pseudospin states $|A\rangle$ and $|B\rangle$,

$$|k\rangle = |A\rangle + \exp(i\varphi_k)|B\rangle, \tag{6}$$

where ϕ_k is the angle of the momentum direction in the graphene plane. Interlayer superconductivity induces partial pairing between the time-reversed momentum states $|k\rangle$ and $|-k\rangle$ located in the Dirac cones of different layers such that the coupling takes place only between the $|A_1\rangle$ and $|B_2\rangle$ pseudospin parts of the electron wave functions in layers 1 and 2, respectively. Since the pairing of the time-reversed chiral momentum states is partial, the interlayer superconductivity (5) gives rise to even parity of the order parameter in the frequency space.[25]

After decoupling of the interacting part of H^{AB} by the order parameter (5), one can diagonalize the Hamiltonian in 2D momentum space. The general expression of the spectrum is large, but for $t_\perp = 0$, we obtain a simple expression for the spectrum $E^{\gamma}_{\mathbf{k}l}$, which is

$$\alpha E^{\gamma}_{\mathbf{k}l} = \alpha\left[\sqrt{\frac{\Delta^2_{\perp 1} + 2\left(\mu^2 + \epsilon^2_{\mathbf{k}}\right) + lA}{2}} - \gamma h\right], \tag{7}$$

$$A = \sqrt{\Delta^4_{\perp 1} + 4\epsilon^2_{\mathbf{k}}\left(\Delta^2_{\perp 1} + 4\mu^2\right)}, \tag{8}$$

where $l, \gamma, \alpha = \pm$ indicate different branches of the spectrum. Here $\epsilon_{\mathbf{k}} = (3/2)t|\mathbf{k}|$, $\mu = (\mu_1 + \mu_2)/2$, and $h = (\mu_1 - \mu_2)/2$ are the free band dispersion, mean doping, and doping difference, respectively. Without loss of generality, we assume $\mu_1 \geqslant \mu_2$. The branch $E^{-}_{\mathbf{k}l}$ does not cross the Fermi surface for any values of the parameters h, μ, $\Delta_{\perp 1}$, and l, such that to break a paired state and send quasiparticles to this state a finite energy is needed. This situation resembles metallic superconductors. Nevertheless, $E^{+}_{\mathbf{k}l}$ can cross the Fermi energy through one point for $l = 1$ and either one or two points for $l = -1$. As a result, it generates gapless excitation modes. In Fig. 2 the quasiparticle excitation spectrum is shown. There are four possible features for $E^{+}_{\mathbf{k}l}$. Each feature, with its own topology of the Fermi surface, can be accessed by tuning the value of h. The boundaries between the four ranges of h associated with different topologies of the Fermi surfaces can be determined by analyzing the roots of $E^{+}_{kl} = 0$; these have three critical values

$$h_{c1} = \mu\sqrt{\frac{\Delta^2_{\perp 1} - t^2_\perp}{\Delta^2_{\perp 1} - t^2_\perp + 4\mu^2}}, \tag{9}$$

$$h_{c2} = \mu, \tag{10}$$

$$h_{c3} = \sqrt{\Delta^2_{\perp 1} - t^2_\perp + \mu^2}. \tag{11}$$

It is easy to see that, in general, $h_{c1} \leqslant h_{c2} \leqslant h_{c1}$.

In the case of $\mu \neq 0$, from Eqs. (9) and (10) one can see that $h_{c1} \neq h_{c2} \neq 0$. In this case, one possible type of Fermi surface topology with no effective Fermi surface for either $l = \pm 1$ occurs when $h < h_{c1}$. In this situation a gap opens and the pairing becomes of BCS type [see Fig. 2(a)]. The value of the energy gap is $2h_{c1}$. But for $\mu = 0$, this regime vanishes and the pairing becomes gapless.

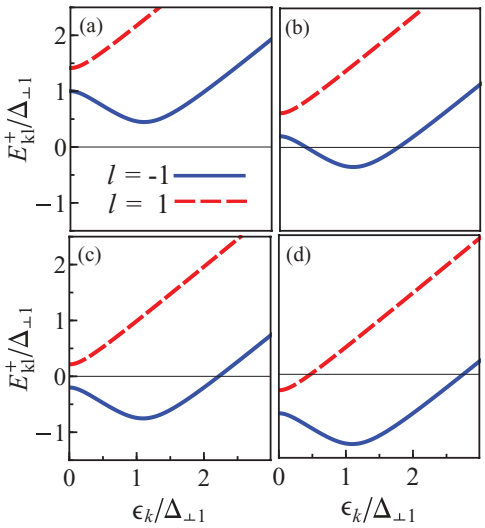

FIG. 2. (Color online) The quasiparticle excitation spectrum E^{+}_{kl} versus ϵ_k in the S state. The dispersions correspond to the regimes of (a) BCS pairing with no effective Fermi surface for both branches $l = \pm 1$, (b) Sarma pairing with two effective Fermi surfaces for the branch $l = -1$ but no Fermi surface for the other branch $l = 1$, (c) pairing with a single Fermi surface in $l = -1$ but no Fermi surface for the other branch $l = 1$, and (d) pn pairing with a single Fermi surface in each branch $l = \pm 1$.

In the range $h_{c1} < h < h_{c2}$ there is a different type of Fermi surface topology. For $l = 1$, there is no effective Fermi surface and the excitation is gapful, whereas the branch $l = -1$ crosses the Fermi level at two points and consequently generates two effective Fermi surfaces, as depicted in Fig. 2(b). This Fermi surface topology corresponds to Sarma pairing in the phase diagram and vanishes at $\mu = 0$.

Another type of Fermi surface topology can be realized for $h_{c2} < h < h_{c3}$. In this range, there is no crossing point between the branch $l = 1$ and the Fermi surface, while the branch $l = -1$ crosses the Fermi surface at one point with a large Fermi momentum. Therefore, as is shown in Fig. 2(c), because of the large Fermi surface, the first excitation band goes to the N state and the second band remains gapped. This topology defines an additional S phase which corresponds to the gapped mixed (GM) regime in the phase diagram.

The last possible Fermi surface topology can be determined when $h_{c3} < h$. In this range, both branches $l = \pm 1$ have one effective Fermi surface [see Fig. 2(d)]. The branch $l = -1$ (1) crosses the Fermi surface with a large (small) Fermi momentum and goes to the N (S) state. It is interesting to note that the splitting of the Fermi surfaces by h in this case results in electronlike and holelike Fermi surfaces in the absence of superconductivity. So the interlayer superconductivity partially pairs n- and p-type momentum states. The corresponding phase will be referred to as the pn phase[26] in the phase diagram.

According to the above four different topologies for the effective Fermi surfaces, the gap equation has different solutions.

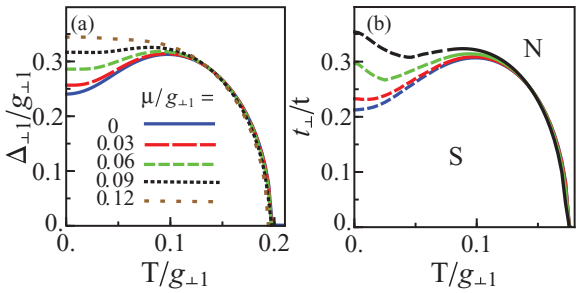

FIG. 3. (Color online) For symmetric doping of bilayer graphene, $h = 0$: (a) The gap solution $\Delta_{\perp 1}$ versus T for different levels of the mean doping μ at $t_\perp = 0$. (b) The mean-field phase diagram of the chiral superconductivity showing the dependence on the interlayer hopping energy $t_\perp$ and the temperature T for $\mu/g_{\perp 1} =$ 0,0.03,0.06,0.09 (from bottom to top, respectively). The line of transition from the N to the S phase is shown, where the dashed and solid parts indicate the first- and second-order transitions, respectively.

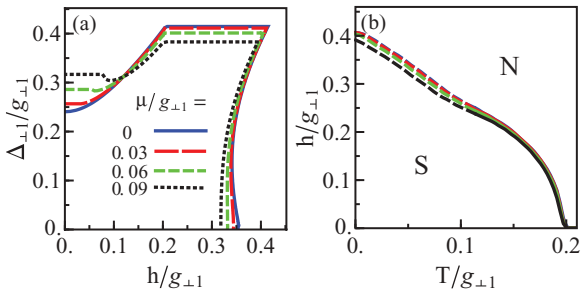

FIG. 4. (Color online) For asymmetric doping of bilayer graphene, $h \neq 0$: (a) TNonzero solutions of the gap equation $\Delta_{\perp 1}$ versus T for different levels of the mean doping μ at $t_\perp = 0$. (b) The mean-field phase diagram of the chiral superconductivity showing dependence on the doping difference h and the temperature T for $\mu/g_{\perp 1} = 0,0.03,0.06,0.09$ (from top to bottom, respectively). The line of transition from the N to the S phase is shown, where the dashed and solid parts indicate the first- and second-order transitions, respectively.

III. INTERLAYER SUPERCONDUCTIVITY IN DOPED BILAYER GRAPHENE

We obtain the gap equation by minimizing the thermodynamic potential

$$\Omega_S = \frac{\Delta_{\perp 1}^2}{g_{\perp 1}} - \frac{1}{\beta}\sum_{\mathbf{k},\gamma,l,\alpha} \ln\left(1 + e^{-\beta\alpha E_{\mathbf{k}l}^{\gamma}}\right) \tag{12}$$

with respect to the order parameters $\Delta_{\perp 1}$ and $\partial\Omega/\partial\Delta_{\perp 1} = 0$. By solving the gap equation self-consistently, one can obtain $\Delta_{\perp 1}$.

For symmetric doping of bilayer graphene, $h = 0$, the solution of the gap equation $\Delta_{\perp 1}$ versus temperature, and the phase diagram of the chiral superconductivity in the $t_\perp$-T plane are shown in Fig. 3 for different levels of the mean doping. In Fig. 3(a), the low-temperature solutions of the gap equation increase with increasing mean doping, and at high mean doping the PA decreases monotonically with temperature, resembling BCS-like behavior. This can be understood as follows: In the absence of doping, the S state is gapless and N fermions will exist as well and this weakens the PA; in the presence of mean doping, a gap opens and the PA strengthens. Finally, for high mean doping, the Fermi surface becomes large and the band structure is not important, as in conventional s-wave symmetry, which results in BCS-like behavior of the PA. The phase diagram of the chiral superconductivity in the $t_\perp$-T plane is shown in Fig. 3(b), and the line of transition from the N to the S phase is shown, where the dashed and solid parts indicate the first- and second-order phase transitions, respectively. One can see that the low-temperature region of the S state increases with the mean doping. This is due to the increase of the PA with the mean doping [shown in Fig. 3(a)]. Since $t_\perp$ normally couples the two layers of the bilayer graphene, larger values of $t_\perp$ are required to cause a larger PA to disappear.

In the case of asymmetrically doped bilayer graphene, $h \neq 0$, the solution of the gap equation $\Delta_{\perp 1}$ versus the doping difference h at zero temperature and the phase diagram of the chiral superconductivity in the h-T plane are shown in Fig. 4 for different levels of the mean doping and $t_\perp = 0$. As depicted in Fig. 4(a), at finite mean doping the behavior of $\Delta_{\perp 1}$ with respect to h is constant up to a certain value h_{c1}, decreases until it develops a minimum at h_{c2}, and then increases; at a critical h, the PA becomes constant and at h_{c3} it abruptly goes to zero. These four steps of behavior of $\Delta_{\perp 1}$ correspond to the four different topologies of the Fermi surface discussed above. Approaching $\mu = 0$, the BCS and Sarma states disappear completely. The phase diagram in the h-T plane is shown in Fig. 4(b), for different levels of the mean doping. The stable S region is separated from the N region by a phase transition line in which the dashed and solid parts indicate the first- and second-order phase transitions, respectively. At low (high) temperature and high (low) doping difference, the phase transition is of first (second) order. By increasing the mean doping, the range of the stable S state is decreased.

In Fig. 5, the phase diagram of the S state in the μ-h plane is shown at zero temperature. The solid thin lines indicate the boundaries of the different phases and the thick dashed line represents the first-order phase transition from the S to the N state. One can see that the BCS, Sarma, and GM phases are stable, while the pn phase is unstable. At $\mu = 0$, the BCS and Sarma states vanish and the only stable state is the GM phase.

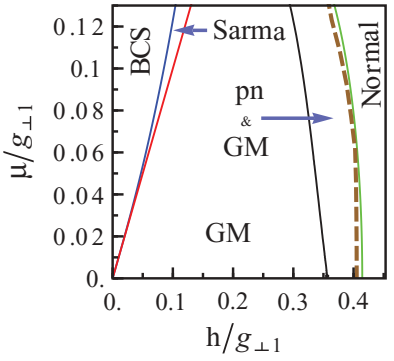

FIG. 5. (Color online) For asymmetric doping of bilayer graphene, $h \neq 0$, the phase diagram of S states in the μ-h plane is shown at zero temperature. Solid thin lines indicate the boundaries of different phases and the thick dashed line represents the first-order phase transition from the S to the N state.

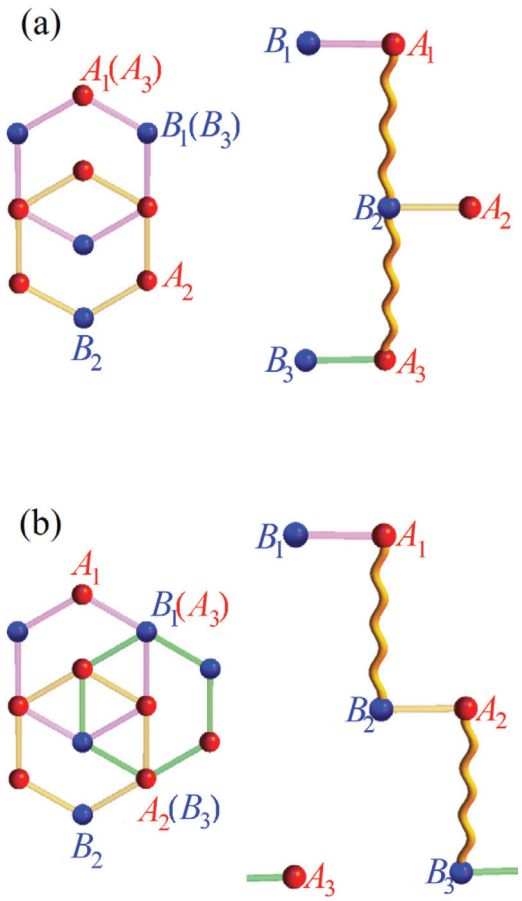

FIG. 6. (Color online) Lattice structure of trilayer graphene. (a) Lattice structure of *ABA*-stacked trilayer graphene in which the sublattices A_1, B_2, and A_3 from different layers are overlapped (left panel). In the right panel, interlayer correlations between electrons of sublattices A_1 and B_2 (B_2 and A_3) from the first and second (second and third) layers are indicated by wavy lines. (b) Lattice structure of *ABC*-stacked trilayer graphene in which the sublattices A_1 and B_2 from the first and second layers and also A_2 and B_3 from the second and third layers are overlapped (left panel). The S correlations between interlayer nearest-neighbor sublattices are shown in the right panel.

Upon increasing μ, the ranges of the BCS and Sarma phases increase, with this property: that the range of the BCS state is larger than that of the Sarma phase.

IV. INTERLAYER SUPERCONDUCTIVITY IN TRILAYER GRAPHENE

In this section, we extend the theory of interlayer superconductivity to the case of trilayer graphene. Trilayer graphene consists of a monolayer graphene on the bottom of the bilayer graphene. There are two known manners of stacking in bulk graphite, which are called *ABA* and *ABC*,[21] as shown in Fig. 6. In *ABA* stacking, the atoms of the bottommost monolayer lie exactly below those of the top layer of the bilayer, while for *ABC* stacking, one type of sublattice of the bottommost monolayer lies under the center of the hexagons in the bottom layer of the bilayer graphene. This subtle difference in stacking order affects the physical properties remarkably. Near the Dirac point, the electrons in *ABC* stacking behave as massive fermions, while in *ABA* stacking, the electrons behave as both massive and massless Dirac fermions.[22] We consider the total Hamiltonian of the π electrons in trilayer graphene without S correlation,[22]

$$H_0^{\rm tri} = \sum_{l=1}^{3} H_l^{\rm mono} + H_\perp^{ABA(C)}, \tag{13}$$

where $H_\perp^{ABA(C)}$ are the nearest-neighbor interlayer hopping Hamiltonians of *ABA*- (*ABC*-) stacked layers and have the following forms:

$$H_\perp^{ABA} = H_\perp^{AB} - t_\perp \sum_{\sigma,i} (b_{2,i,\sigma}^\dagger a_{3,i,\sigma} + \text{H.c.}), \tag{14}$$

$$H_\perp^{ABC} = H_\perp^{AB} - t_\perp \sum_{\sigma,i} (a_{2,i,\sigma}^\dagger b_{3,i,\sigma} + \text{H.c.}). \tag{15}$$

To induce interlayer superconductivity, we introduce the nearest-neighbor interlayer attractive interaction

$$V_\perp^{ABA} = V_\perp^{AB} - g_{\perp 2} \sum_{\sigma,\sigma',i} b_{2,i,\sigma}^\dagger b_{2,i,\sigma} a_{3,i,\sigma'}^\dagger a_{3,i,\sigma'} \tag{16}$$

for the *ABA* trilayer and

$$V_\perp^{ABC} = V_\perp^{AB} - g_{\perp 2} \sum_{\sigma,\sigma',i} a_{2,i,\sigma}^\dagger a_{2,i,\sigma} b_{3,i,\sigma'}^\dagger b_{3,i,\sigma'} \tag{17}$$

for *ABC* trilayer graphene. $g_{\perp 2}$ couples the electrons of the sublattice B_2 (A_2) and A_3 (B_3) in the *ABA* (*ABC*) arrangement. The first terms of Eqs. (16) and (17) can be decoupled by Eq. (5). Following the discussion of Sec. II, we determine the S order parameters between the second and the third layers,

$$\Delta_{i,\perp 2} = -g_{\perp 2} \langle b_{2,i,\downarrow} a_{3,i,\uparrow} + b_{2,i,\uparrow} a_{3,i,\downarrow} \rangle \tag{18}$$

for decoupling the second term of Eq. (16) and

$$\Delta_{i,\perp 2} = -g_{\perp 2} \langle a_{2,i,\downarrow} b_{3,i,\uparrow} + a_{2,i,\uparrow} b_{3,i,\downarrow} \rangle \tag{19}$$

for decoupling the second term of Eq. (17). In momentum space, the total Hamiltonian of trilayer graphene ($H^{ABA(C)} = H_0^{\rm tri} + V_\perp^{ABA(C)}$) can be diagonalized. With the procedure of Sec. III, we can calculate the PAs for different stackings of the trilayer. Figure 7 shows the nonzero stable solutions of $\Delta_{\perp 1}$ and $\Delta_{\perp 2}$ in terms of temperature for pure *ABA* and *ABC* trilayers at $t_\perp = 0$. As in the bilayer case, there is an enhancement of the

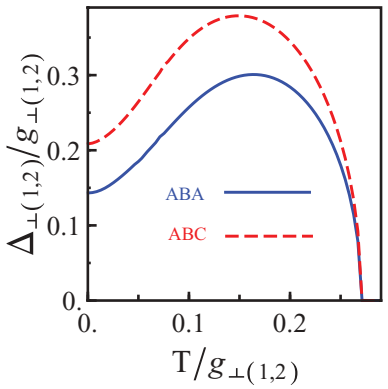

FIG. 7. (Color online) Solutions of gap equations $\Delta_{\perp(1,2)}$ versus temperature for *ABA* and *ABC* stacking at $\mu = 0$ and $t_\perp = 0$.

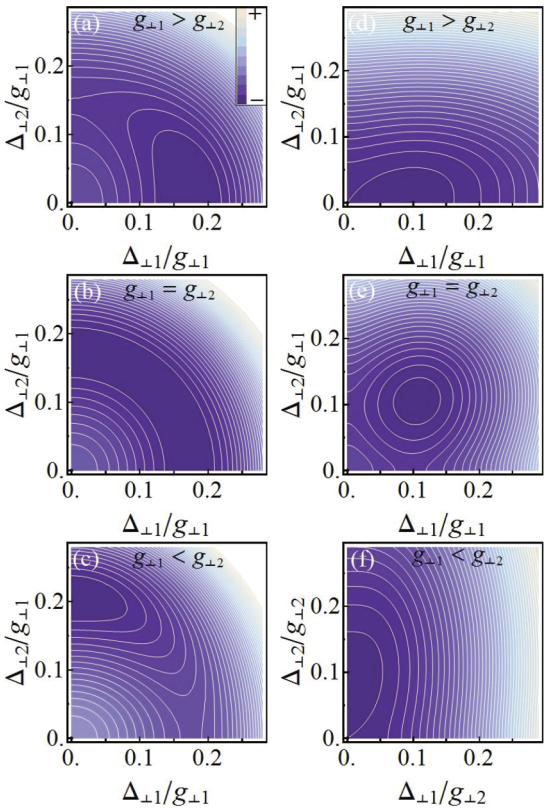

FIG. 8. (Color online) Finite-temperature thermodynamic potential contours in the $\Delta_{\perp 1}$-$\Delta_{\perp 2}$ plane showing stable points. In the case of *ABA* stacking, steps (a) $g_{\perp 1} > g_{\perp 2}$ ($g_{\perp 1}/g_{\perp 2} = 1.02$), (b) $g_{\perp 1} = g_{\perp 2}$, and (c) $g_{\perp 1} < g_{\perp 2}$ ($g_{\perp 1}/g_{\perp 2} = 0.98$) indicate first-order phase transitions between $\Delta_{\perp 1}$ and $\Delta_{\perp 2}$, whereas in the case of *ABC* stacking, steps (d) $g_{\perp 1} > g_{\perp 2}$ ($g_{\perp 1}/g_{\perp 2} = 3.11$), (e) $g_{\perp 1} = g_{\perp 2}$, and (f) $g_{\perp 1} < g_{\perp 2}$ ($g_{\perp 1}/g_{\perp 2} = 0.32$) imply that second-order phase transitions occur.

PA at intermediate temperatures. However, the values of the *ABC* trilayer order parameter are larger than those of the *ABA* trilayer, and as a result, in this case, the simultaneous existence of $\Delta_{\perp 1}$ and $\Delta_{\perp 2}$ promotes the interlayer superconductivity. We will discuss below the case of *ABA* stacking. It is interesting to note that there is a mutual influence between the interlayer PAs. The manner of the effect strongly depends on the type of layer arrangement. This effect can be investigated by studying the competition between $\Delta_{\perp 1}$ and $\Delta_{\perp 2}$ with respect to the relative values of $g_{\perp 1}$ and $g_{\perp 2}$. In Fig. 8, a contour plot of the thermodynamic potential in the $\Delta_{\perp 1}$-$\Delta_{\perp 2}$ plane for *ABA*- and *ABC*-stacked layers is shown for $\mu = 0$ and $t_\perp = 0$. In the *ABA* trilayer graphene, if $g_{\perp 1} > g_{\perp 2}$, the global (local) minimum of the thermodynamic potential lies on the $\Delta_{\perp 1}$ ($\Delta_{\perp 2}$) axis [see Fig. 8(a)]. On increasing $g_{\perp 2}$ so that $g_{\perp 1} = g_{\perp 2}$, the thermodynamic potential shows many stationary points where the global minimum is a quarter of a circle as shown in Fig. 8(b). This behavior of the global minimum is due to the symmetry of the parameter space. On further increase of $g_{\perp 2}$, so that $g_{\perp 1} < g_{\perp 2}$, the minimum of the thermodynamic potential passes to a nonzero $\Delta_{\perp 2}$ but zero $\Delta_{\perp 1}$ [see Fig. 8(c)]. On the other hand, on varying $g_{\perp 1}$ and $g_{\perp 2}$, the stable point jumps between the two axes, implying a first-order phase transition between $\Delta_{\perp 1}$ and $\Delta_{\perp 2}$. The situation for the *ABC* trilayer is different. Figure 8(d) shows that if $g_{\perp 1} > g_{\perp 2}$, the dominant PA is $\Delta_{\perp 1}$ and the other has a small value. On the other hand, the thermodynamic potential has one point of the global minimum without a local minimum. This stationary point moves continually in the $\Delta_{\perp 1}$-$\Delta_{\perp 2}$ plane on variation of $g_{\perp 1}$ and $g_{\perp 2}$. At the same values of $g_{\perp 1}$ and $g_{\perp 2}$, the PAs have equal magnitude [see Fig. 8(e)]. Finally, $\Delta_{\perp 2}$ will be larger than $\Delta_{\perp 1}$ if $g_{\perp 1} < g_{\perp 2}$, as is shown in Fig. 8(f). Therefore, changing the $g_\perp$'s exhibits a second-order phase transition between the order parameters.

V. CONCLUSION

In conclusion, we have analyzed in bilayer and trilayer graphene *s*-wave spin-triplet superconductivity, which can be realized by an interlayer pairing between chiral electrons of different layers. For bilayer graphene, we have shown that the gapless property of the interlayer S state of a pure sample and its associated temperature-induced enhancement of the S order parameter are suppressed by finite mean doping. We have explored the possibility of realizing four distinct pairing regimes with different topologies of the Fermi surfaces by tuning the difference in the doping levels of the two layers. These include the BCS regime in which the two relevant branches of excitations are gapped and S [Fig. 2(a)], the Sarma regime with one branch gapped and the other gapless, both S [Fig. 2(b)], the gapped mixed regime with one branch gapped and S and the other N [Fig. 2(c)], and the *pn* regime with both branches being gapless, one S and the other N [Fig. 2(d)].

For trilayer graphene, we have shown that the interlayer pairing strongly depends on the type of stacking, with *ABC* stacking supporting a higher pairing amplitude than *ABA* stacking. For imbalanced coupling strengths of the middle layer with the two outer layers, we distinguish two phases which are characterized by the pairing of the middle layer with only one of the outer layers. We have found a phase transition between these two phases by varying the ratio of the coupling strengths; the transition is first order for the *ABA* stacking but second order for the *ABC* stacking.

ACKNOWLEDGMENTS

The authors gratefully acknowledge support by the Institute for Advanced Studies in Basic Sciences (IASBS) Research Council under Grant No. G2012IASBS110. M.Z. thanks ICTP in Trieste for hospitality and support during his visit to this institute.

[1] J. Bardeen, L. N. Cooper, and J. R. Schriffer, Phys. Rev. **108**, 1175 (1957).
[2] F. Wilczek, Mod. Phys. Lett. A **25**, 3169 (2010).
[3] M. W. Zwierlein, A. Schirotzek, C. H. Schunck, and W. Ketterle, Science **311**, 492 (2006); G. B. Partridge, W. Li, R. I. Kamar, Y.-A. Liao, and R. G. Hulet, *ibid.* **311**, 503 (2006); G. B. Partridge,

Wenhui Li, Y. A. Liao, R. G. Hulet, M. Haque, and H. T. C. Stoof, Phys. Rev. Lett. **97**, 190407 (2006).

[4]A. Sedrakian, J. Mur-Petit, A. Polls, and H. Muther, Phys. Rev. A **72**, 013613 (2005); C.-H. Pao, S.-T. Wu, and S.-K. Yip, Phys. Rev. B **73**, 132506 (2006); D. E. Sheehy and L. Radzihovsky, Phys. Rev. Lett. **96**, 060401 (2006); J. Dukelsky, G. Ortiz, S. M. A. Rombouts, and K. Van Houcke, *ibid.* **96**, 180404 (2006); P. Pieri and G. C. Strinati, *ibid.* **96**, 150404 (2006); J. Kinnunen, L. M. Jensen, and P. Torma, *ibid.* **96**, 110403 (2006); F. Chevy, *ibid.* **96**, 130401 (2006); K. Machida, T. Mizushima, and M. Ichioka, *ibid.* **97**, 120407 (2006); M. Haque and H. T. C. Stoof, Phys. Rev. A **74**, 011602(R) (2006).

[5]M. Alford, K. Rajagopal, and F. Wilczek, Nucl. Phys. B **537**, 443 (1999); Mark G. Alford, Krishna Rajagopal, Thomas Schaefer, and Andreas Schmitt, Rev. Mod. Phys. **80**, 1455 (2008); M. Alford, J. A. Bowers, and K. Rajagopal, Phys. Rev. D **63**, 074016 (2001); I. Shovkovy and M. Huang, Phys. Lett. B **564**, 205 (2003); M. Alford, C. Kouvaris, and K. Rajagopal, Phys. Rev. Lett. **92**, 222001 (2004).

[6]A. Sedrakian and U. Lombardo, Phys. Rev. Lett. **84**, 602 (2000); for a review, see A. Sedrakian, J. W. Clark, and M. G. Alford, *Pairing in Fermionic Systems: Basic Concepts and Modern Applications* (World Scientific, Singapore, 2006).

[7]M. Tinkham, *Introduction to Superconductivity* (Dover, New York, 2004).

[8]G. Sarma, J. Phys. Chem. Solids **24**, 1029 (1963); W. V. Liu and F. Wilczek, Phys. Rev. Lett. **90**, 047002 (2003); E. Gubankova, W. V. Liu, and F. Wilczek, *ibid.* **91**, 032001 (2003); Michael McNeil Forbes, E. Gubankova, W. V. Liu, and F. Wilczek, *ibid.* **94**, 017001 (2005).

[9]H. Muther and A. Sedrakian, Phys. Rev. Lett. **88**, 252503 (2002).

[10]P. Fulde and R. A. Ferrell, Phys. Rev. **135**, A550 (1964); A. I. Larkin and Y. N. Ovchinnikov, Zh. Eksp. Teor. Fiz. **47**, 1136 (1964) [Sov. Phys. JETP **20**, 762 (1965)]; R. Casalbuoni and G. Nardulli, Rev. Mod. Phys. **76**, 263 (2004).

[11]Warren E. Pickett, Rev. Mod. Phys. **61**, 433 (1989); Andrea Damascelli, Zahid Hussain, and Zhi-Xun Shen, *ibid.* **75**, 473 (2003); C. C. Tsuei and J. R. Kirtley, *ibid.* **72**, 969 (2000); D. N. Basov and T. Timusk, *ibid.* **77**, 721 (2005).

[12]A. J. Leggett, Nat. Phys. **2**, 134 (2006); Y. Kamihara, H. Hiramatsu, M. Hirano, R. Kawamura, H. Yanagi, T. Kamiya, and H. Hosono, J. Am. Chem. Soc. **128**, 31 (2006); Y. Kamihara, T. Watanabe, M. Hirano, and H. Hosono, *ibid.* **130**, 3296 (2008); H. Takahashi, K. Igawa, K. Arii, Y. Kamihara, M. Hirano, and H. Hosono, Nature (London) **453**, 376 (2008); G. R. Stewart, Rev. Mod. Phys. **83**, 1589 (2011).

[13]K. S. Novoselov, A. K. Geim, S. V. Morozov, D. Jiang, Y. Zhang, S. V. Dubonos, I. V. Grigorieva, and A. A. Firsov, Science **306**, 666 (2004).

[14]K. S. Novoselov, A. K. Geim, S. V. Morozov, D. Jiang, M. I. Katsnelson, I. V. Grigorieva, S. V. Dubonos, and A. A. Firsov, Nature (London) **438**, 197 (2005); Y. B. Zhang, Y. W. Tan, H. L. Stormer, and P. Kim, *ibid.* **438**, 201 (2005); A. K. Geim and K. S. Novoselov, Nat. Mater. **6**, 183 (2007).

[15]A. M. Black-Schaffer and S. Doniach, Phys. Rev. B **75**, 134512 (2007); J. L. McChesney, A. Bostwick, T. Ohta, T. Seyller, K. Horn, J. Gonzalez, and E. Rotenberg, Phys. Rev. Lett. **104**, 136803 (2010); Bitan Roy and Igor F. Herbut, Phys. Rev. B **82**, 035429 (2010); Sandeep Pathak, Vijay B. Shenoy, and G. Baskaran, *ibid.* **81**, 085431 (2010); Matthias Einenkel and Konstantin B. Efetov, *ibid.* **84**, 214508 (2011); Rahul Nandkishore, L. S. Levitov, and A. V. Chubukov, Nat. Phys. **8**, 158 (2012); Maximilian L. Kiesel, Christian Platt, Werner Hanke, Dmitry A. Abanin, and Ronny Thomale, Phys. Rev. B **86**, 020507 (2012).

[16]Bruno Uchoa and A. H. Castro Neto, Phys. Rev. Lett. **98**, 146801 (2007).

[17]C. W. J. Beenakker, Rev. Mod. Phys. **80**, 1337 (2008); A. H. Castro Neto, F. Guinea, N. M. R. Peres, K. S. Novoselov, and A. K. Geim, *ibid.* **81**, 109 (2009).

[18]Thomas E. Weller, Mark Ellerby, Siddharth S. Saxena, Robert P. Smith, and Neal T. Skipper, Nat. Phys. **1**, 39 (2005); N. Emery, C. Hérold, M. d'Astuto, V. Garcia, C. Bellin, J. F. Marêche, P. Lagrange, and G. Loupias, Phys. Rev. Lett. **95**, 087003 (2005).

[19]Hubert B. Heersche, Pablo Jarillo-Herrero, Jeroen B. Oostinga, Lieven M. K. Vandersypen, and Alberto F. Morpurgo, Nature (London) **446**, 56 (2007); F. Miao, S. Wijeratne, Y. Zhang, U. C. Coskun, W. Bao, and C. N. Lau, Science **317**, 1530 (2007).

[20]M. V. Hosseini and M. Zareyan, Phys. Rev. Lett. **108**, 147001 (2012).

[21]W. J. Zhu, V. Perebeinos, M. Freitag, and P. Avouris, Phys. Rev. B **80**, 235402 (2009); Y. P. Liu, S. Goolaup, C. Murapaka, W. S. Lew, and S. K. Wong, ACS Nano **4**, 7087 (2010); K. F. Mak, J. Shan, and T. F. Heinz, Phys. Rev. Lett. **104**, 176404 (2010); W. Bao, L. Jing, J. Velasco, Jr., Y. Lee, G. Liu, D. Tran, B. Standley, M. Aykol, S. B. Cronin, D. Smirnov, M. Koshino, E. McCann, M. Bockrath, and C. N. Lau, Nat. Phys. **7**, 948 (2011).

[22]F. Guinea, A. H. Castro Neto, and N. M. R. Peres, Phys. Rev. B **73**, 245426 (2006); S. Latil and L. Henrard, Phys. Rev. Lett. **97**, 036803 (2006); C. L. Lu, C. P. Chang, Y. C. Huang, R. B. Chen, and M. L. Lin, Phys. Rev. B **73**, 144427 (2006); B. Partoens and F. M. Peeters, *ibid.* **74**, 075404 (2006); M. Aoki and H. Amawashi, Solid State Commun. **142**, 123 (2007); F. Guinea, Phys. Rev. B **75**, 235433 (2007); M. Koshino and E. McCann, *ibid.* **80**, 165409 (2009); Fan Zhang, Bhagawan Sahu, Hongki Min, and A. H. MacDonald, *ibid.* **82**, 035409 (2010).

[23]E. McCann and V. I. Falko, Phys. Rev. Lett. **96**, 086805 (2006).

[24]G. Baskaran, Phys. Rev. B **65**, 212505 (2002).

[25]F. S. Bergeret, A. F. Volkov, and K. B. Efetov, Rev. Mod. Phys. **77**, 1321 (2005).

[26]M. V. Hosseini and M. Zareyan, arXiv:1209.3727 (2012).